iScience

CellPress

Article

Efficient CO_2 Utilization via a Hybrid Na-CO_2 System Based on CO_2 Dissolution

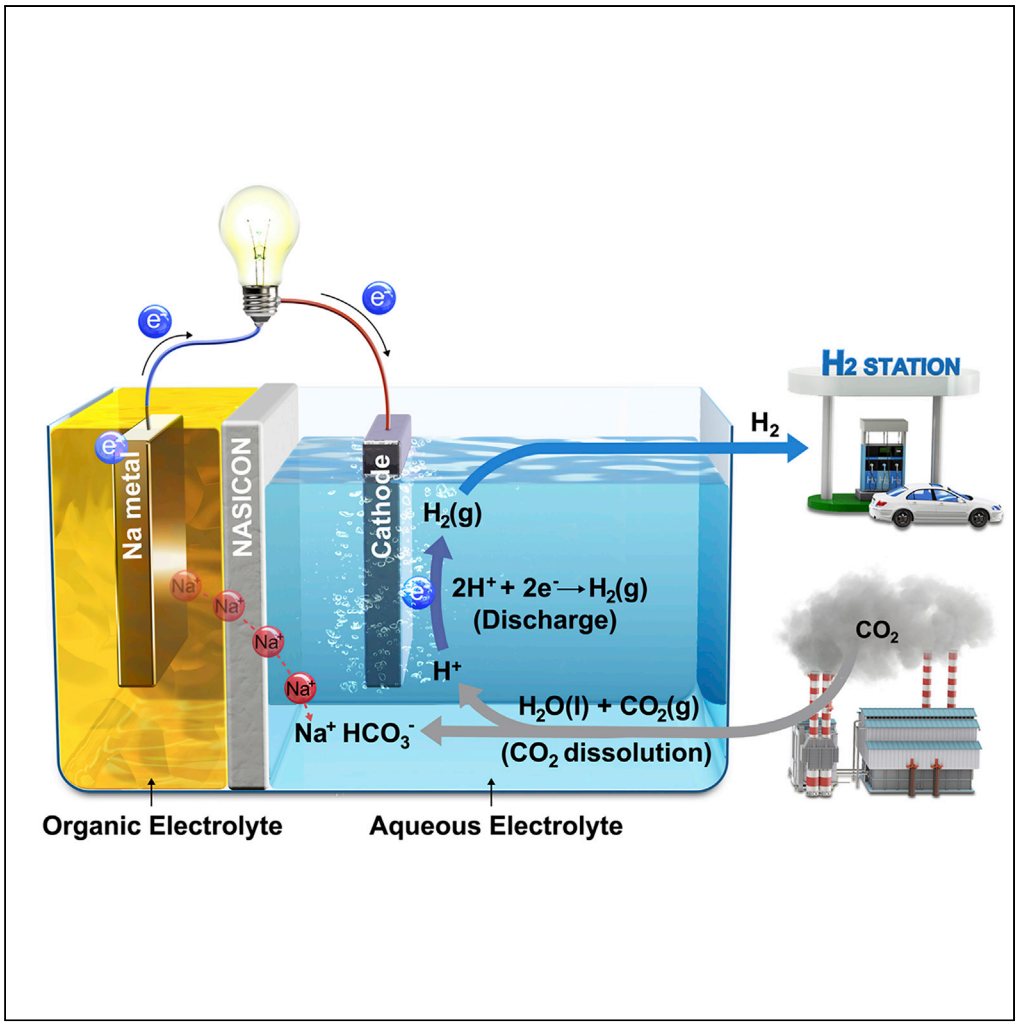

Changmin Kim, Jeongwon Kim, Sangwook Joo, Yunfei Bu, Meilin Liu, Jaephil Cho, Guntae Kim

jpcho@unist.ac.kr (J.C.)
gtkim@unist.ac.kr (G.K.)

HIGHLIGHTS

Hybrid Na-CO_2 cell continuously produces electricity and H_2 through CO_2 conversion

Hybrid Na-CO_2 does not regenerate CO_2 during charging, unlike aprotic metal-CO_2 cells

Highly stable operation over 1,000 hr was achieved with CO_2 utilization

Kim et al., iScience 9, 278–285
November 30, 2018
https://doi.org/10.1016/j.isci.2018.10.027

iScience

CellPress

Article

Efficient CO_2 Utilization via a Hybrid Na-CO_2 System Based on CO_2 Dissolution

Changmin Kim,[1,4] Jeongwon Kim,[1,4] Sangwook Joo,[1] Yunfei Bu,[2] Meilin Liu,[3] Jaephil Cho,[1,*] and Guntae Kim[1,5,*]

SUMMARY

Carbon capture, utilization, and sequestration technologies have been extensively studied to utilize carbon dioxide (CO_2), a greenhouse gas, as a resource. So far, however, effective technologies have not been proposed owing to the low efficiency conversion rate and high energy requirements. Here, we present a hybrid Na-CO_2 cell that can continuously produce electrical energy and hydrogen through efficient CO_2 conversion with stable operation for over 1,000 hr from spontaneous CO_2 dissolution in aqueous solution. In addition, this system has the advantage of not regenerating CO_2 during charging process, unlike aprotic metal-CO_2 cells. This system could serve as a novel CO_2 utilization technology and high-value-added electrical energy and hydrogen production device.

INTRODUCTION

Many researchers believe that global warming and climate change are the result of carbon dioxide (CO_2) generated by human activities over the centuries (Jenkinson et al., 1991; Obama, 2017). Thus, many countries and organizations have made great efforts to reduce their carbon footprint, and recently, the carbon capture, utilization, and storage/sequestration (CCUS) technology has been studied to recycle CO_2 as a resource (Keith et al., 2018; Andersen, 2017; Dowell et al., 2017). In this regard, considerable research has been focused on the chemical conversion of CO_2 into high-value-added carbon compounds, such as methanol, organic materials, and plastics (Liu et al., 2015; Li et al., 2016; Angamuthu et al., 2010; Darensbourg, 2007). However, owing to the low conversion efficiency, it has been pointed out that it cannot be an effective greenhouse gas abatement technology (Bourzac, 2017; Markewitz et al., 2012; Mikkelsen et al., 2010). Recently, aprotic (non-aqueous) metal-CO_2 batteries have also been studied for the production of electrical energy using CO_2 (Zhang et al., 2015; Qie et al., 2017; Hu et al., 2016; Al Sadat and Archer, 2016; Das et al., 2013). However, during the generation of electric energy, solid carbonate products accumulate on the surface of the electrode, which deteriorates the performance and discharge capacity. In addition, because CO_2 is regenerated in the charging process, aprotic metal-CO_2 batteries are not an efficient CCUS technology for utilizing and reducing CO_2. Thus, we have devised a hybrid Na-CO_2 battery that continuously produces electric energy and hydrogen simultaneously through efficient CO_2 conversion with highly stable operation over 1,000 hr from the nature of spontaneous CO_2 dissolution in an aqueous solution. We further show that unlike existing aprotic metal-CO_2 batteries (Zhang et al., 2015; Qie et al., 2017; Hu et al., 2016; Al Sadat and Archer, 2016), the proposed system does not regenerate CO_2 during the charging process. Therefore, this hybrid Na-CO_2 cell, which adopts efficient CCUS technologies, not only utilizes CO_2 as the resource for generating electrical energy but also produces the clean energy source, hydrogen.

RESULTS AND DISCUSSION

The Proposed Hybrid Na-CO_2 Cell and Its Reaction Mechanism

A schematic illustration of the proposed hybrid Na-CO_2 cell is presented in Figure 1. The digital photographs of the system are also presented in Figure S1. This system could work continuously with Na metal and CO_2 as fuel at the anode and feedstock gas at the cathode, respectively. Na is regarded as a promising candidate as a substitute for Li in terms of its electrochemically similar behavior along with low cost (30 times cheaper than Li) from natural abundance and environmental friendliness (Noorden, 2014; Kwak et al., 2015). The Na metal anode is kept in an organic electrolyte to prevent a direct corrosion from an aqueous electrolyte separating by Na super ionic conductor (NASICON) membrane. The overall reaction mechanisms are composed of a chemical reaction and an electrochemical reaction.

The chemical reaction of CO_2 dissolution mechanism is as follows:

$$CO_2(aq) + H_2O(l) \rightleftharpoons H_2CO_3(aq),\ K_h = 1.70 \times 10^{-3} \quad \text{(Equation 1)}$$

[1]Department of Energy Engineering, Ulsan National Institute of Science and Technology (UNIST), Ulsan 44919, Republic of Korea

[2]School of Environment Science and Engineering, Nanjing University of Information Science and Technology (NUIST), Nanjing, Jiangsu, 210044, China

[3]School of Materials Science & Engineering, Georgia Institute of Technology, Atlanta, GA 30332-0245, USA

[4]These authors contributed equally

[5]Lead Contact

*Correspondence: jpcho@unist.ac.kr (J.C.), gtkim@unist.ac.kr (G.K.)

https://doi.org/10.1016/j.isci.2018.10.027

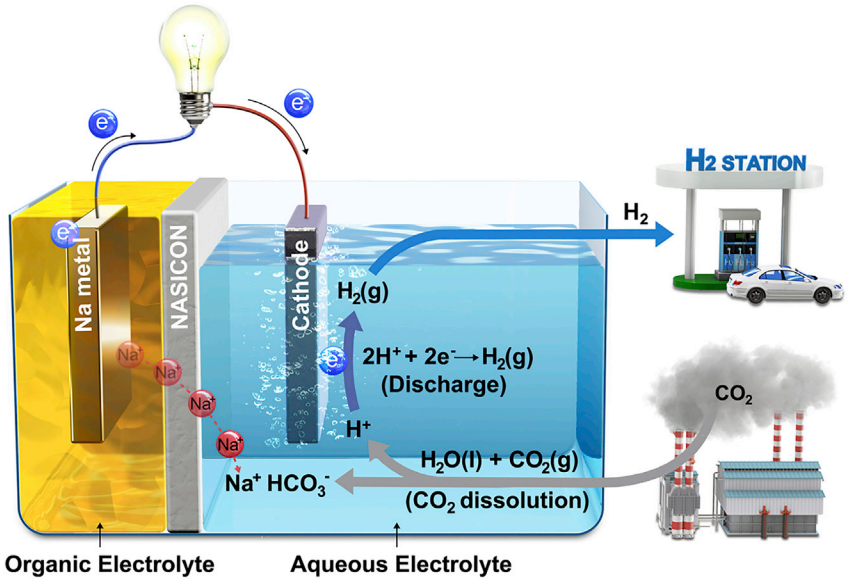

Figure 1. Schematic Illustration of Hybrid Na-CO_2 System and its Reaction Mechanism

$$H_2CO_3(aq) \rightleftharpoons HCO_3^-(aq) + H^+(aq),\ pK_{a1} = 6.3 \qquad \text{(Equation 2)}$$

When CO_2 is purged into an aqueous solution (*e.g.*, distilled water, seawater, NaOH solution), CO_2 dissolution proceeds and carbonic acid (H_2CO_3(aq)) is formed through the hydration of CO_2 (Equation 1). For a standard state condition in pure water, this spontaneous chemical equilibrium of CO_2 hydration is determined by the hydration equilibrium constant ($K_h = 1.70 \times 10^{-3}$) (Housecroft and Sharpe, 2005). Then, the carbonic acid dissociates into HCO_3^- and H^+ determined by the first acid dissociation constant ($K_{a1} = 4.46 \times 10^{-7}$), shown in Equation 2 (Harris, 2010). Because carbonic acid is a polyprotic acid dissociating multiple steps, an in-depth understanding of CO_2 dissolution requires that the second acid dissociation step, *i.e.*, $HCO_3^-(aq) \rightleftharpoons CO_3^{2-}(aq) + H^+(aq)$ ($K_{a2} = 4.69 \times 10^{-11}$), be considered (Harris, 2010). However, the second acid dissociation constant is significantly smaller than the first ($K_{a1} >> K_{a2}$), making it negligible in calculating the proton concentration. Thus, when CO_2 dissolved in water, it acidifies the aqueous solution and $HCO_3^-(aq)$ is predominant over $CO_3^{2-}(aq)$. The concentration of carbonate ions when CO_2 dissolves in water at normal atmospheric pressure is provided at Table S1. The mole fractions of carbonate ions depending on the pH of solution is shown in Figure S2.

The electrochemical reactions are composed of anodic reaction of sodium metal oxidation (Equation 3) and cathodic reaction of hydrogen evolution (Equation 4):

$$\text{Anodic reaction: } 2Na \rightarrow 2Na^+ + 2e^-\ E^o = -2.71\ V \qquad \text{(Equation 3)}$$

$$\text{Cathodic reaction: } 2H^+ + 2e^- \rightarrow H_2(g)\ E^o = 0.00\ V \qquad \text{(Equation 4)}$$

$$\text{Net equation: } 2Na + 2H^+ \rightarrow 2Na^+ + H_2(g)\ E^o = 2.71\ V \qquad \text{(Equation 5)}$$

Then, the electrochemical net equation is simply given as the oxidation of Na metal and the spontaneous evolution of hydrogen (Equation 5). Because the potential of cathodic reaction is closely influenced by the pH of aqueous solution, the dissolution of CO_2 renders a favorable electrochemical reaction environment by acidifying the aqueous solution.

Half-Cell Configured Electrochemical Analysis

The cathodic electrochemical profiles were closely examined using a cyclic voltammetry (CV) technique on the Pt electrode (Figure 2A). An apparent cathodic peak in O_2-saturated NaOH was observed

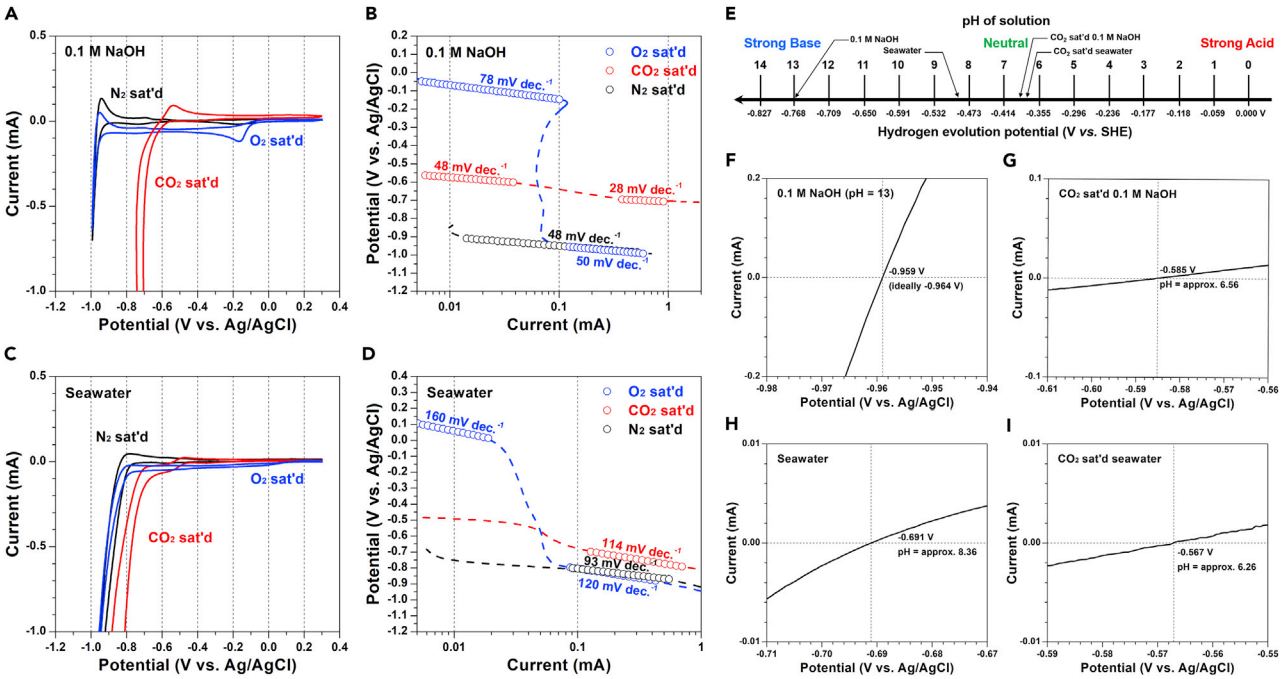

Figure 2. Half-Cell Configured Electrochemical Analysis

(A) Cathodic CV profiles measured in O_2-, N_2-, and CO_2-saturated 0.1 M NaOH at 10 mV s^{-1}, using Pt as the working and counter electrode and Ag/AgCl electrode as the reference electrode. A reference potential is described with Ag/AgCl instead of reversible hydrogen electrode (RHE) for the clarification of potential difference with respect to purging gases and pH.

(B) Tafel analysis of the cathodic profiles.

(C) Cathodic CV profiles measured in O_2- and CO_2-saturated seawater.

(D) Corresponding Tafel plots.

(E–I) (E) Schematic diagram of hydrogen evolution potential related to pH. RHE calibration profile corresponding to hydrogen evolution potential measured in (F) 0.1 M NaOH, (G) CO_2-saturated 0.1 M NaOH, (H) seawater, and (I) CO_2-saturated seawater.

near of −0.1 V versus Ag/AgCl, which could be ascribed to an oxygen reduction reaction (ORR) on the Pt electrode (Park et al., 1986; Kim et al., 2016). When ORR occurred, a diffusion-controlled region was found near of −0.2 V and a limiting current was observed due to the typical O_2 mass transfer limitation in ORR profiles (Kim et al., 2016; Bu et al., 2017). At the lower potential, a cathodic peak corresponding to hydrogen evolution reaction (HER) was observed around −0.95 V in O_2- and N_2-saturated conditions (Mahmood et al., 2017; Xu et al., 2016; Ahn et al., 2018). Meanwhile, in the case of CO_2-saturated condition, hydrogen evolution occurs more positively by 0.35 V due to the higher concentration of H^+. In addition, HER profiles, contrary to ORR profiles, presented sharply increasing cathodic curves without a mass transfer limitation. For depth analysis, the kinetics of these electrochemical reactions were interpreted by an analysis of the Tafel slope (Figure 2B). Because ORR is one of the most complex electrochemical reactions, involving 4 electrons with 2 reactants (O_2 and H_2O), the reaction kinetics is sluggish, even on a state-of-the-art Pt electrode, with a value of 78 mV $dec.^{-1}$. However, HER only involves 2 electrons with 1 reactant (H^+ or H_2O depending on the pH) and thus presented a low Tafel slope of 48 mV $dec.^{-1}$ near the onset potential. Furthermore, the Tafel slope is more decreased to 28 mV $dec.^{-1}$ at an activation-controlled Tafel region, indicating a highly efficient cathodic reaction. Furthermore, the cathodic CVs and the corresponding Tafel plots were investigated in seawater (Figures 2C and 2D). Likewise, it has been confirmed that CO_2 dissolution in seawater provides the electrochemically favorable environment toward HER. The hydrogen evolution potential based on pH is described in Figures 2E–2I. These electrochemical profiles have significant implications; the less corrosive environment of the quasi-neutral condition (pH ~ 7) could potentially allow the adoption of abundant and non-noble-metal-based electrocatalysts. Thus, notably, this combined cathodic reaction not only utilizes CO_2 to generate H_2 but also possesses highly efficient reaction kinetics, possibly overcoming the key issue of sluggish discharge rates for common metal-air batteries (Wang et al., 2014).

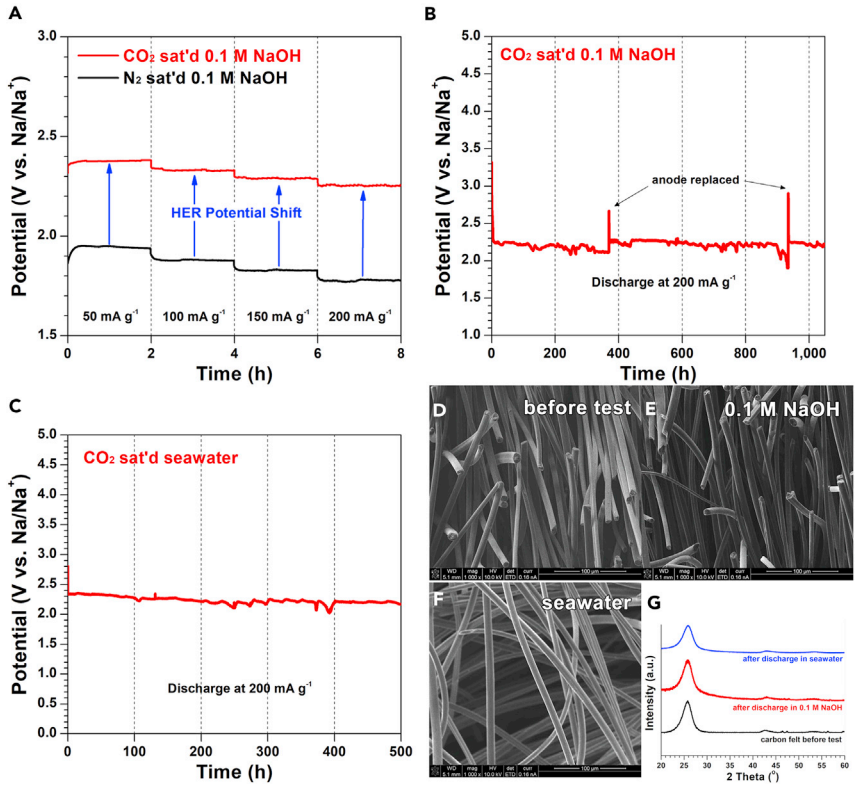

Figure 3. Performance and Stability of Hybrid Na-CO_2 Cell

(A) Chronopotentiometric potential profiles on the hybrid Na-CO_2 system under various current densities. Discharge processes are conducted in CO_2- and N_2-saturated 0.1 M NaOH to observe the effects of CO_2 dissolution.

(B and C) (B) The chronopotentiometric discharge profile of Pt/C + IrO_2 catalyst at 200 mA g^{-1} in CO_2-saturated 0.1 M NaOH. (C) Discharge profile of hybrid Na-CO_2 system measured in CO_2-saturated seawater. Surface observation of carbon felt cathode before and after test.

(D–F) (D) Scanning electron micrograph of carbon felt before and (E) after discharge in 0.1 M NaOH and (F) after discharge in seawater.

(G) XRD profiles of carbon felt electrode before and after discharge in 0.1 M NaOH and seawater.

Performance and Stability of Hybrid Na-CO_2 Cell

The actual working performance of a hybrid Na-CO_2 cell is evaluated using a composite of Pt/C and IrO_2 (Pt/C + IrO_2) as a catalyst. Figure 3A presents the chronopotentiometric discharge profiles at a current density of 50–200 mA g^{-1} under N_2- or CO_2-saturated 0.1 M NaOH. Discharging CV profiles measured in various gas-saturated conditions were also investigated, and three distinctive reduction peaks were found, as observed in the half-cell CV profiles (Figure S3). These findings confirmed that the dissolution of CO_2 led to a favorable HER environment in both NaOH solution and seawater. The full discharge profile was investigated in a CO_2-saturated NaOH solution (Figure 3B) with a mechanical recharge by replacing the Na metal anode. As shown in Figure 3B, the highly stable operation over 1,000 hr was achieved because only a gas phase H_2(g) was produced during the discharge process, suggesting the similar nature of fuel cell systems (Park et al., 2000; Sengodan et al., 2015; Yang et al., 2009). Also, the full discharge profile measured under CO_2-saturated seawater presented a highly stable operation over 500 hr (Figure 3C). In other words, there is no deposition of solid discharge products that possibly causes clogging or physical damage on the electrode as examined from scanning electron micrographs and X-ray diffraction (XRD) patterns (Figures 3D–3G). In contrast, conventional aprotic metal-CO_2 batteries have exhibited typical clogging phenomenon by the deposition of solid M_2CO_3(s) (M = Li or Na), $Al_2(C_2O_4)_3$(s), or $MgCO_3$(s) on the surface of the electrode (Zhang et al., 2015; Qie et al., 2017; Hu et al., 2016; Al Sadat and Archer, 2016; Das et al., 2013), which results in a performance drop with limited capacity. A comparison of the capacities of various batteries is provided in Table S2. Furthermore, the pH

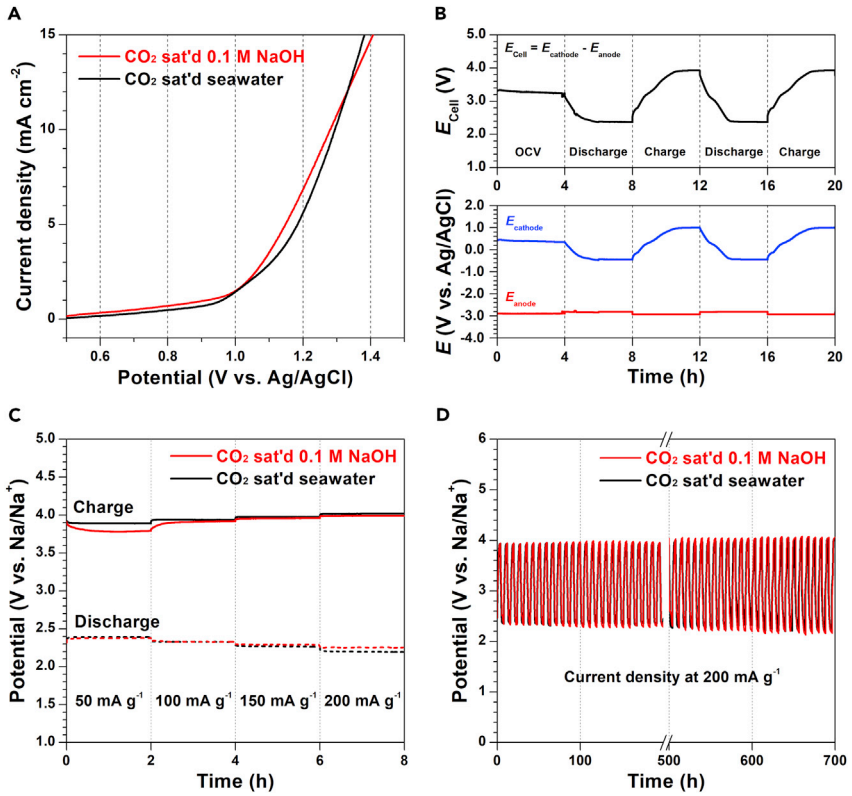

Figure 4. Reversibility of Hybrid Na-CO_2 Cell

(A) Anodic rotating disk electrode profile of Pt/C + IrO_2 catalyst measured in CO_2-saturated 0.1 M NaOH and seawater at 10 mV s^{-1}, using Pt as a counter electrode and Ag/AgCl electrode as a reference electrode.

(B) Discharge-charge profiles measured in three-electrode configuration using Ag/AgCl reference electrode at 100 mA g^{-1}.

(C) Charge-discharge profiles at various current densities under CO_2-saturated 0.1 M NaOH and seawater.

(D) Cyclic charge-discharge performance measured in CO_2-saturated 0.1 M NaOH and seawater at a current density of 200 mA g^{-1} for 700 hr.

of the CO_2-saturated NaOH solution after the 1,000-hr operation was investigated and determined to be 6.62, indicating that the pH of the solution is stably maintained over 1,000 hr (Figure S4). The produced gas during operation was analyzed by gas chromatography (GC), which confirms that this system generates only H_2, as expected from Equation 4, during the discharge process (Figure S5). To identify a soluble product, the aqueous solution was freeze-dried and obtained in the form of a white powder (the inset of Figure S6). The XRD patterns of the white powder identifies it as pure $NaHCO_3$ (Figure S6), commonly known as baking soda. It is notable that the continuous enrichment of $NaHCO_3$(aq) in the aqueous media from the discharge does not affect the discharge performance, as shown in the 1,000-hr discharge profile (Figure 3B). Therefore, CO_2 gas has been successfully captured and converted to baking soda. The additional XRD profiles of the powder obtained through different drying processes are provided in Figure S7. Furthermore, we investigated the practical CO_2 conversion efficiency through quantitative GC analysis. As shown in Figure S8, the practical efficiency of CO_2 conversion during the discharge reaction was determined to be 47.7%. Although this value is lower than the theoretical conversion rate, it is meaningful in that it proves the additional CO_2 dissolution during the discharge process. The detailed discussion is available in Supplemental Information.

Reversibility of Hybrid Na-CO_2 Cell

To confirm the reversibility of hybrid Na-CO_2 cell, the anodic charge profile (electrolysis profile) was observed. Because Na is one of the most abundant elements on earth, Na metal anode could be easily recycled through a charging process in Na-ion-containing aqueous solution, such as seawater. Figure 4A shows an oxidation rotating disk electrode profile for examining whether CO_2 was reproduced during

the charging process. Generally, the charging process is regarded as the opposite reaction of the discharging reaction. In this work, however, the generated H_2 gas from the discharging process is naturally removed on the surface of electrode, and thus the oxidation reaction proceeds as the oxygen evolution reaction (OER) from the water oxidation (Equation 6).

$$2H_2O \rightarrow O_2(g) + 4H^+ + 4e^- \quad E^o = 1.229\ V \qquad \text{(Equation 6)}$$

The oxidation curve corresponding to OER (Kim et al., 2016; Bu et al., 2017) was observed in a CO_2-saturated NaOH solution near 1.0 V versus Ag/AgCl (from the Nernst equation, the OER potential can be calibrated by 0.0592 V × pH). In addition, the qualitative GC profiles indicate that O_2 was generated during the oxidation process (Figures S9 and S10). We further investigated the oxidation profiles in seawater, which presents the typical chlorine evolution reaction (Kim et al., 2015) instead of OER (Figure 4A). It is noteworthy that the charging process does not generate CO_2, which had already been consumed during discharge, as opposed to the conventional metal-CO_2 battery system, which emits CO_2 during the charging process (Zhang et al., 2015; Qie et al., 2017; Hu et al., 2016; Al Sadat and Archer, 2016). The discharge-charge performance of this system was evaluated in the three-electrode configuration using Ag/AgCl reference electrode to closely distinguish the potential applied on the cathode and anode (Figure 4B). Since a cell potential (E_{cell}) is defined as a potential difference of cathode and anode ($E_{cathode} - E_{anode}$), the potential gap decreases during discharging and increases during the charging process. On repeating the discharge-charge process, the cathode potential profile ($E_{cathode}$) presents discharging and charging plateau, clearly proving that this system is rechargeable. Furthermore, the charge-discharge profiles at various current densities under CO_2-saturated NaOH solution and seawater are examined as shown in Figure 4C. Cyclic charge-discharge performance was evaluated to verify its reversibility and reproducibility (Figure 4D). Both cyclic performances were highly reproducible and obtained without variations over a period of 700 hr, indicating that H_2 is stably produced utilizing CO_2 and that the cathode was kept fresh, without clogging or damage, during a repeating discharge and charge process.

In summary, we have devised hybrid Na-CO_2 cell utilizing CO_2 as a useful resource. This new system has three distinctive advantages. First, it uses a kinetically fast HER as a discharge reaction thanks to a spontaneous CO_2 dissolution, enabling the provision of high current compared with the present aprotic system. Second, unlike conventional aprotic CO_2 batteries, wherein solid products are clogged on the electrodes, this system can continuously produce gas-phase hydrogen during discharge without damaging the electrode. This ability enabled highly stable performance to be achieved over 1,000 hr. Third, the proposed system has the unprecedented great advantage of not regenerating CO_2 while recycling Na metal through charging process. Therefore, this hybrid Na-CO_2 cell truly fulfills the purpose of a real CCUS technology, as it consumes CO_2 efficiently throughout the process. This novel system could potentially serve as a new CO_2 utilization technology and a stepping stone for the future utilization of renewable energy technologies.

Limitations of Study

We have devised hybrid Na-CO_2 cell utilizing carbon dioxide as a useful resource. Although we have utilized HER as the facile cathodic reaction rather than ORR in aqueous electrolyte, we could not exclude the fact that the discharge reaction of hybrid Na-CO_2 cell is relatively slow because of the low conductivity of the ceramic NASICON electrolyte, which can allow only Na^+ ions to pass through. The present work indicates the novel hydrogen generation technology from CO_2 utilization and is meaningful in that it proves the additional CO_2 dissolution during the discharge process, but further work is required to improve the CO_2 conversion efficiency and power densities of the hybrid Na-CO_2 cell.

METHODS

All methods can be found in the accompanying Transparent Methods supplemental file.

SUPPLEMENTAL INFORMATION

Supplemental Information includes Transparent Methods, 10 figures, 2 tables and can be found with this article online at https://doi.org/10.1016/j.isci.2018.10.027.

ACKNOWLEDGMENTS

This research was supported by the Mid-Career Researcher Program (NRF-2018R1A2A1A05077532) through the National Research Foundation of Korea, funded by the Ministry of Science, ICT and Future Planning. It was also supported by the Korea CCS R&D Center (KCRC) grant (NRF-2017M1A8A1072054). This research was also supported by Natural Science Foundation of Jiangsu Province (BK20160834).

AUTHOR CONTRIBUTIONS

C.K. and J.K. contributed equally to this work. C.K. and J.K. performed the experiments, data analysis, and experimental planning. S.J. conducted the GC measurement and analysis. C.K., J.K., Y.B., J.C., and G.K. discussed the results and analyzed the data. M.L. and J.C. provided thoughtful comments and edited the manuscript. The work was conceived, planned, and supervised by G.K. All authors contributed to writing the manuscript.

DECLARATION OF INTERESTS

The authors declare no competing interests.

Received: September 1, 2018
Revised: September 30, 2018
Accepted: October 26, 2018
Published: November 30, 2018

REFERENCES

Ahn, W., Park, M.G., Lee, D.U., Seo, M.H., Jiang, G., Cano, Z.P., Hassan, F.M., and Chen, Z. (2018). Hollow multivoid nanocuboids derived from ternary Ni-Co-Fe prussian blue analog for dual-electrolysis of oxygen and hydrogen evolution reactions. Adv. Funct. Mater. *28*, 1802129.

Al Sadat, W.I., and Archer, L.A. (2016). The O_2-assisted Al/CO_2 electrochemical cell: a system for CO_2 capture/conversion and electric power generation. Sci. Adv. *2*, e1600968.

Andersen, S.O. (2017). We can and must govern climate engineering. Nature *551*, 415.

Angamuthu, R., Byers, P., Lutz, M., Spek, A.L., and Bouwman, E. (2010). Electrocatalytic CO_2 conversion to oxalate by a copper complex. Science *327*, 313–315.

Bourzac, K. (2017). We have the technology. Nature *550*, S66–S69.

Bu, Y., Gwon, O., Nam, G., Jang, H., Kim, S., Zhong, Q., Cho, J., and Kim, G. (2017). A highly efficient and robust cation ordered perovskite oxide as a bifunctional catalyst for rechargeable Zinc-air batteries. ACS Nano *11*, 11594–11601.

Darensbourg, D.J. (2007). Making plastics from carbon dioxide: salen metal complexes as catalysts for the production of polycarbonates from epoxides and CO_2. Chem. Rev. *107*, 2388–2410.

Das, S.K., Xu, S., and Archer, L.A. (2013). Carbon dioxide assist for non-aqueous sodium-oxygen batteries. Electrochem. Commun. *27*, 59–62.

Dowell, N.M., Fennell, P.S., Shah, N., and Maitland, G.C. (2017). The role of CO_2 capture and utilization in mitigating climate change. Nat. Clim. Chang. *7*, 243–249.

Harris, D.C. (2010). Quantitative Chemical Analysis, Eight edition (W. H. Freeman and Company).

Housecroft, C.E., and Sharpe, A.G. (2005). Inorganic Chemistry, Second edition (Pearson Prentice Hall).

Hu, X., Sun, J., Li, Z., Zhao, Q., Chen, C., and Chen, J. (2016). Rechargeable room-temperature Na-CO2 batteries. Angew. Chem. Int. Ed. *55*, 6482–6486.

Jenkinson, D.S., Adams, D.E., and Wild, A. (1991). Model estimates of CO_2 emissions from soil in response to global warming. Nature *351*, 304–306.

Keith, D.W., Holmes, G., Angelo, D.St., and Heidel, K. (2018). A process for capturing CO_2 from the atmosphere. Joule *2*, 1573–1594.

Kim, J.-K., Lee, E., Kim, H., Johnson, C., Cho, J., and Kim, Y. (2015). Rechargeable seawater battery and its electrochemical mechanism. ChemElectroChem *2*, 328–332.

Kim, C., Gwon, O., Jeon, I.-Y., Kim, Y., Shin, J., Ju, Y.-W., Baek, J.-B., and Kim, G. (2016). Cloud-like graphene nanoplatelets on $Nd_{0.5}Sr_{0.5}CoO_{3-\delta}$ nanorods as an efficient bifunctional electrocatalyst for hybrid Li-air batteries. J. Mater. Chem. A *4*, 2122–2127.

Kwak, W.-J., Chen, Z., Yoon, C.S., Lee, J.-K., Amine, K., and Sun, Y.-K. (2015). Nanoconfinement of low-conductivity products in rechargeable sodium-air batteries. Nano Energy *12*, 123–130.

Li, P.-Z., Wang, X.-J., Liu, J., Lim, J.S., Zou, R., and Zhao, Y. (2016). A triazole-containing metal-organic framework as a highly effective and substrate size-dependent catalyst for CO_2 conversion. J. Am. Chem. Soc. *138*, 2142–2145.

Liu, C., Yang, B., Tyo, E., Seifert, S., DeBartolo, J., Issendorff, B.v., Zapol, P., Vajda, S., and Curtiss, L.A. (2015). Carbon dioxide conversion to methanol over size-selected Cu_4 clusters at low pressures. J. Am. Chem. Soc. *137*, 8676–8679.

Mahmood, J., Li, F., Jung, S.-M., Okyay, M.S., Ahmad, I., Kim, S.-J., Park, N., Jeong, H.Y., and Baek, J.-B. (2017). An efficient and pH-universal ruthenium-based catalyst for the hydrogen evolution reaction. Nat. Nanotechnol. *12*, 441–446.

Markewitz, P., Kuckshinrichs, W., Leitner, W., Linssen, J., Zapp, P., Bongartz, R., Schreiber, A., and Müller, T.E. (2012). Worldwide innovations in the development of carbon capture technologies and the utilization of CO_2. Energy Environ. Sci. *5*, 7281–7305.

Mikkelsen, M., Jørgensen, M., and Krebs, F.C. (2010). The teraton challenge. A review of fixation and transformation of carbon dioxide. Energy Environ. Sci. *3*, 43–81.

Noorden, R.V. (2014). A better battery. Nature *507*, 26–28.

Obama, B. (2017). The irreversible momentum of clean energy. Science *355*, 126–129.

Park, S.-M., Ho, S., Aruliah, S., Weber, M.F., Ward, C.A., and Venter, R.D. (1986). Electrochemical reduction of oxygen at platinum electrodes in KOH solution – temperature and concentration effects. J. Electrochem. Soc. *133*, 1641–1649.

Park, S., Vohs, J.M., and Gorte, R.J. (2000). Direct oxidation of hydrocarbon in a solid-oxide fuel cell. Nature *404*, 265–267.

Qie, L., Lin, Y., Connell, J.W., Xu, J., and Dai, L. (2017). Highly rechargeable lithium-CO_2 batteries with a boron- and nitrogen-codoped holey-graphene cathode. Angew. Chem. Int. Ed. *56*, 6970–6974.

Sengodan, S., Choi, S., Jun, A., Shin, T.H., Ju, Y.-W., Jeong, H.Y., Shin, J., Irvine, J.T.S., and Kim, G. (2015). Layered oxygen-deficient double

perovskite as an efficient and stable anode for direct hydrocarbon solid oxide fuel cells. Nat. Mater. *14*, 205–209.

Wang, Z.-L., Xu, D., Xu, J.-J., and Zhang, X.-B. (2014). Oxygen electrocatalysts in metal-air batteries: from aqueous to nonaqueous electrolytes. Chem. Soc. Rev. *43*, 7746–7786.

Xu, X., Chen, Y., Zhou, W., Zhu, Z., Su, C., Liu, M., and Shao, Z. (2016). A perovskite electrocatalyst for efficient hydrogen evolution reaction. Adv. Mater. *28*, 6442–6448.

Yang, L., Wang, S., Blinn, K., Liu, M., Liu, Z., Cheng, Z., and Liu, M. (2009). Enhanced sulfur and coking tolerance of a mixed ion conductor for SOFCs: $BaZr_{0.1}Ce_{0.7}Y_{0.2-x}Yb_xO_{3-\delta}$. Science *326*, 126–129.

Zhang, Z., Zhang, Q., Chen, Y., Bao, J., Zhou, X., Xie, Z., Wei, J., and Zhou, Z. (2015). The first introduction of graphene to rechargeable Li-CO_2 batteries. Angew. Chem. Int. Ed. *54*, 6550–6553.

ISCI, Volume *9*

Supplemental Information

Efficient CO_2 Utilization via a Hybrid Na-CO_2 System Based on CO_2 Dissolution

Changmin Kim, Jeongwon Kim, Sangwook Joo, Yunfei Bu, Meilin Liu, Jaephil Cho, and Guntae Kim

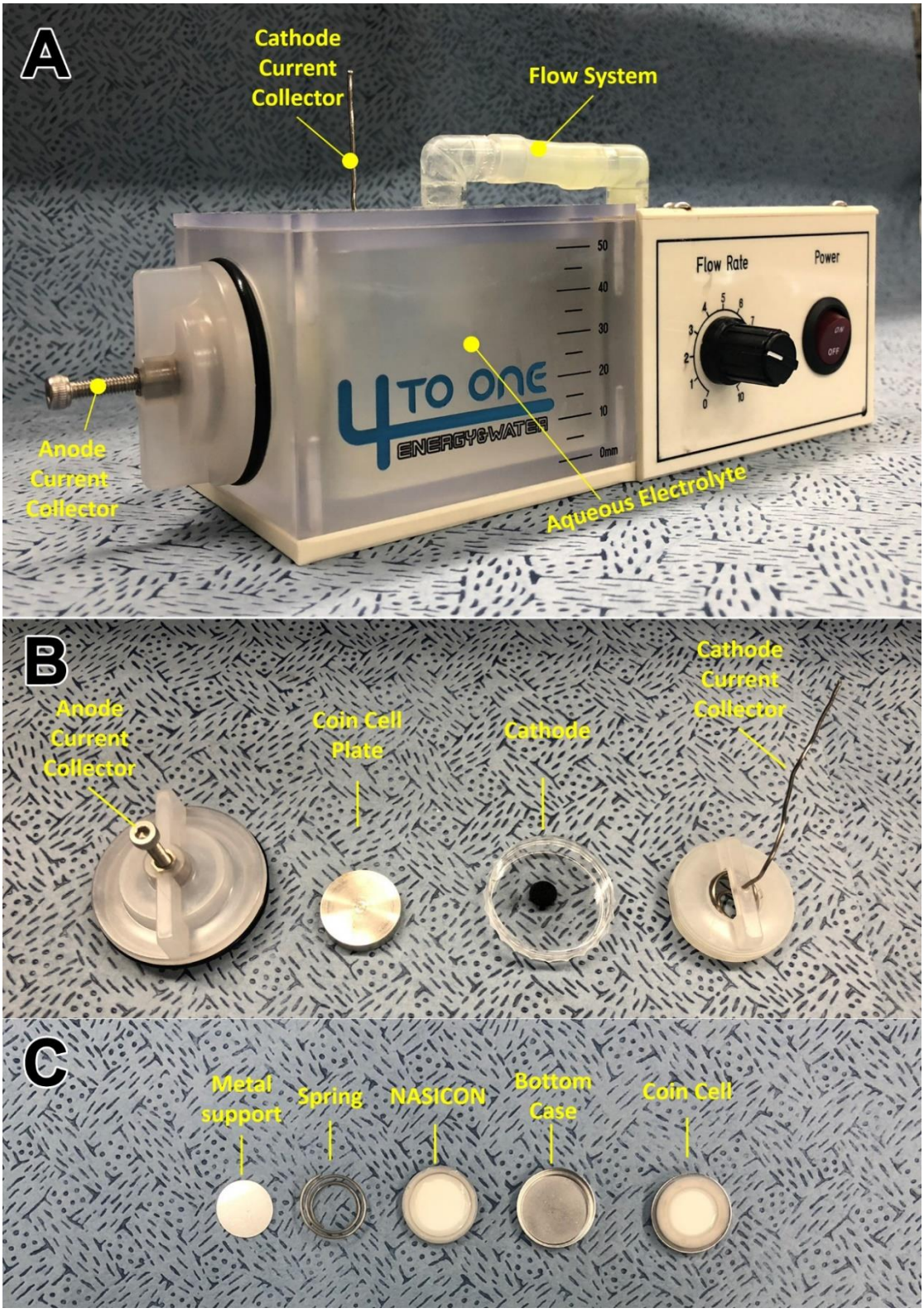

Figure S1. The components of hybrid Na-CO_2 cell. Related to Figure 1. (A) The digital photograph of hybrid Na-CO_2 cell. (B) The anode and cathode assembly of Na -CO_2 cell. (C) The components of anode coin cell. Details are available in Transparen t Methods. Related to Figure 1.

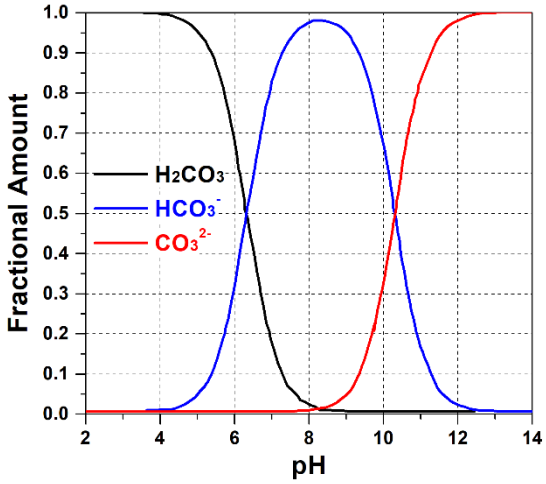

Figure S2. Mole fractions of the three different carbonate forms, *i.e.*, carbonic acid ion, bicarbonate ion, and carbonate ion, as a function of pH of dissolved solution (Note: carbonic acid ion here includes ionic carbon dioxide). Related to Figure 1.

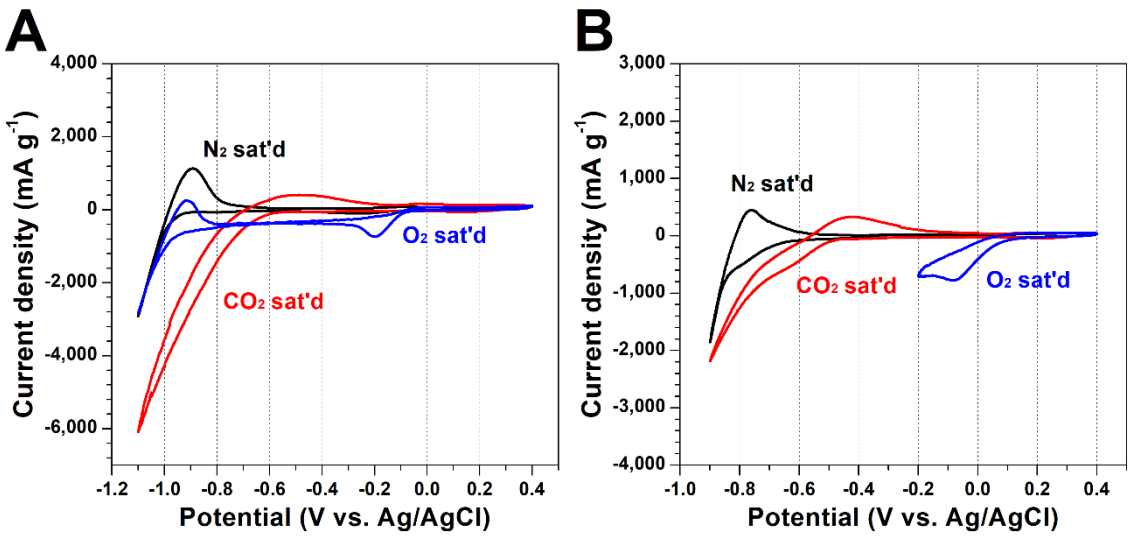

Figure S3. Cathodic full-cell CV profiles measured by Pt/C+IrO_2 catalyst at 0.1 mV s^{-1} in the hybrid Na-CO_2 system conducted in three-electrode configuration using Ag/AgCl. Related to Figure 3. CV profiles measured in O_2, N_2, or CO_2 saturated (A) 0.1 M NaOH (B) seawater. These profiles reveal the CO_2 dissolution could render a favorable electrochemical environment to HER.

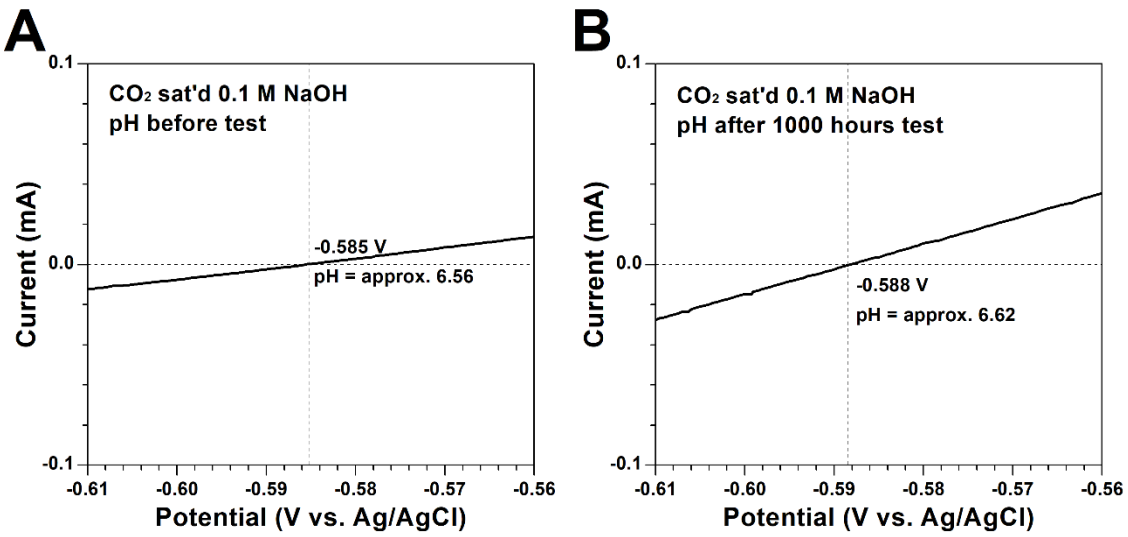

Figure S4. The pH of the CO_2-saturated 0.1 M NaOH solution. Related to Figure 2. (A) before test and (B) after 1000 hours test.

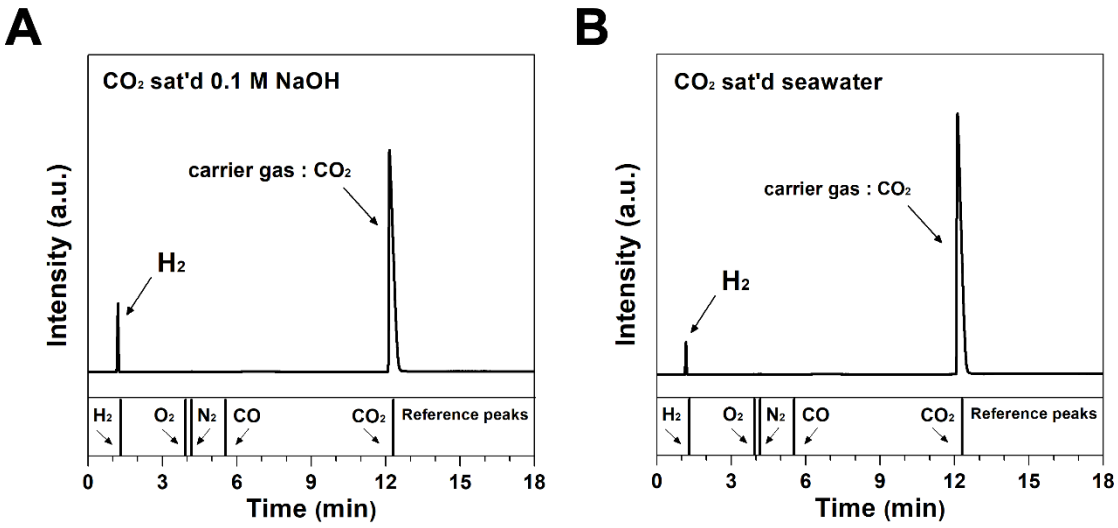

Figure S5. Gas chromatography (GC) profiles of generated gas during discharge process, Related to Figure 3. The gas obtained during cathodic reaction proceeded in (A) CO_2 saturated 0.1 M NaOH (B) CO_2 saturated seawater.

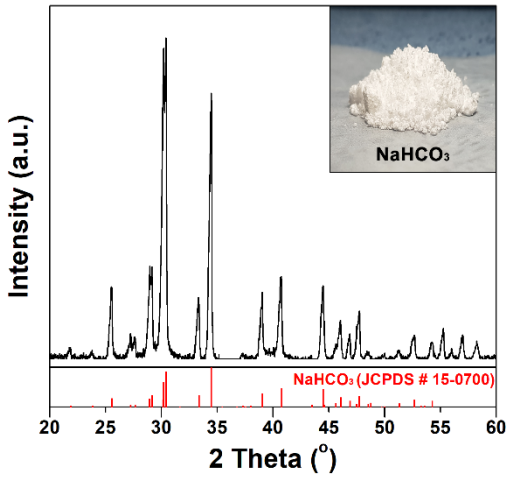

Figure S6. XRD profile of the solidified aqueous solution *via* freeze-drying. Related to Figure 3. The inset shows the obtained white powder.

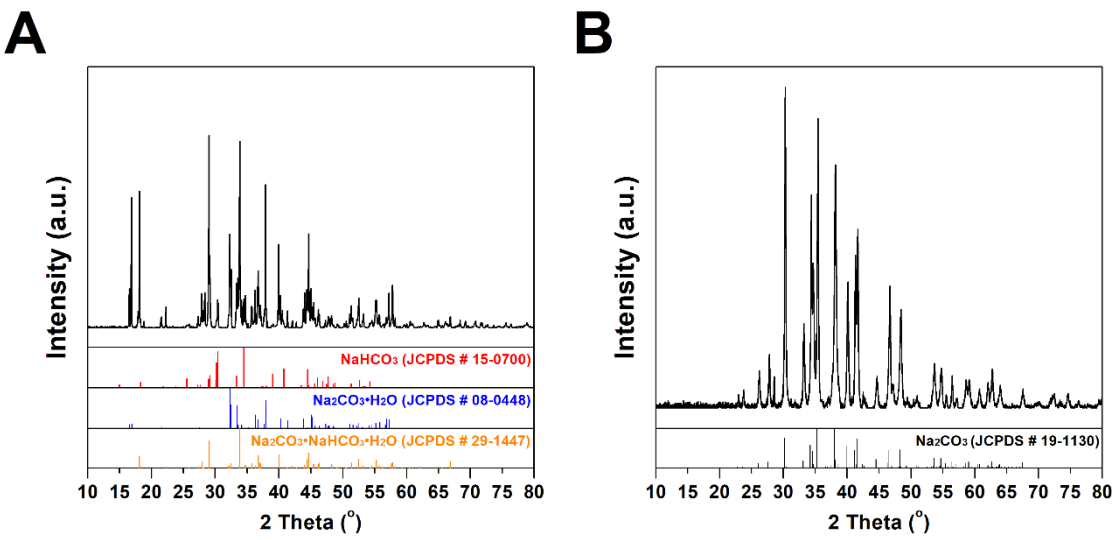

Figure S7. XRD profiles of the soluble product after discharge reaction obtained by various drying conditions. Related to Figure 3. (A) Dried at room temperature. Because non-marine evaporites precipitate in different proportions of chemical elements from those found in the aqueous environments, three different minerals (nahcolite: $NaHCO_3$, thermonatrite: $Na_2CO_3 \cdot H_2O$, and trona: $Na_2CO_3 \cdot NaHCO_3 \cdot 2H_2O$) are naturally obtained. (B) Dried at 70 ºC oven. Only Na_2CO_3 is formed when dried at high temperature.

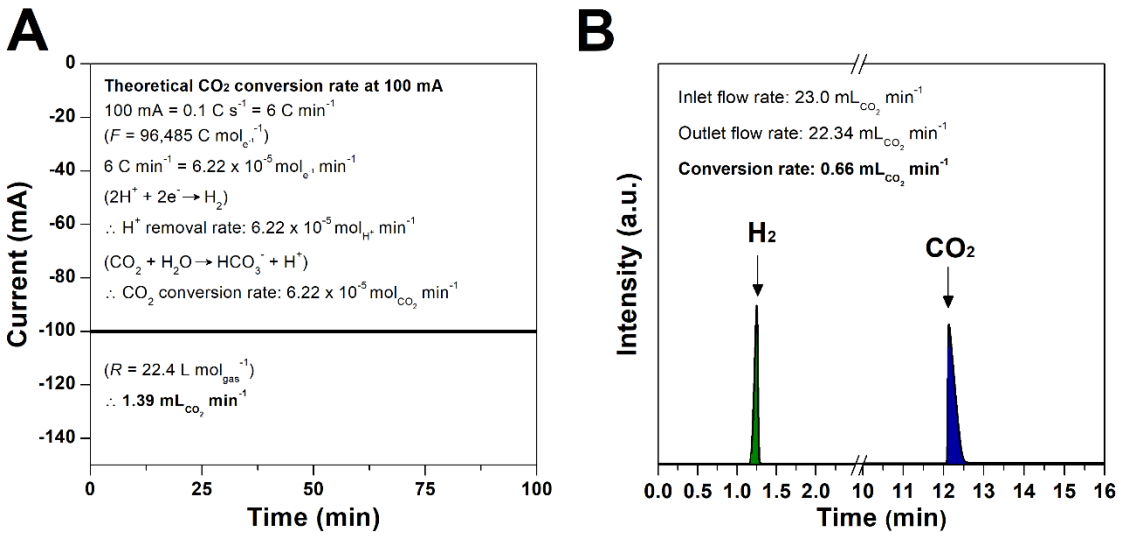

Figure S8. The experimental CO_2 conversion efficiency. Related to Figure 3. (A) Theoretical CO_2 conversion rate at current of 100 mA. (B) The quantitative GC profiles of outlet CO_2 gas during practical measurement condition for different inlet CO_2 flow rate of 23.0 mL min^{-1}.

We have determined the efficiency of CO_2 conversion during the reaction time. First, theoretical CO_2 conversion rate is determined by calculating H^+ removal rate during discharge reaction. Because one CO_2 molecule can make one H^+ molecule from the dissolution process (*i.e.,* $CO_2 + H_2O \rightarrow H^+ + HCO_3^-$) and two H^+ molecules can make one H_2 molecule (*i.e.*, $2H^+ + 2e^- \rightarrow H_2$), we can assume two CO_2 molecules can contribute to produce one H_2 molecule (100 % conversion efficiency). As shown in **Figure S8A**, the theoretical CO_2 conversion rate is determined at the current of 100 mA, *i.e.*, 1.39 mL min^{-1}. Then, the quantitative GC profiles of outlet CO_2 gas during discharge reaction have been examined. As shown in **Figure S8B**, the measurement proceeds at the inlet CO_2 flow rate of 23.0 mL min^{-1} and the outlet CO_2 flow rate was 22.34 mL min^{-1}. Accordingly, the practically converted CO_2 rate is determined, *i.e.*, 0.66 mL min^{-1}. Thus, the practical efficiencies of CO_2 conversion were calculated to be 47.7 %. Although this value is lower than the theoretical conversion rate, it is meaningful in that proves the additional CO_2 dissolution during the discharge process. It is also expected that the time that CO_2 contacts the solution (*i.e.*, it related to the depth of the solution.) will also affect the conversion rate.

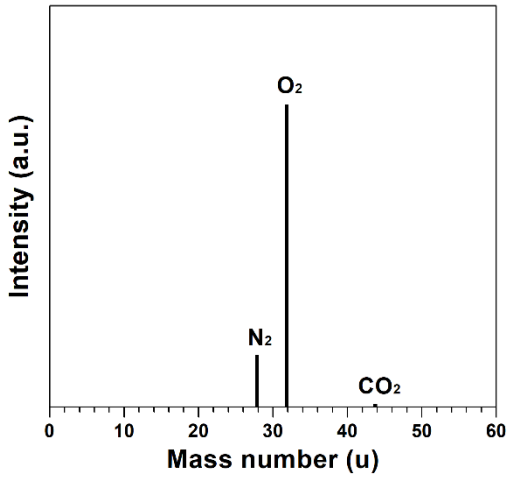

Figure S9. The GC profile of generated gas during the oxidation process. Related to Figure 4 and Figure S10. The data indicates a generation of O_2 gas (In detailed GC profiles are available in **Figure S10**).

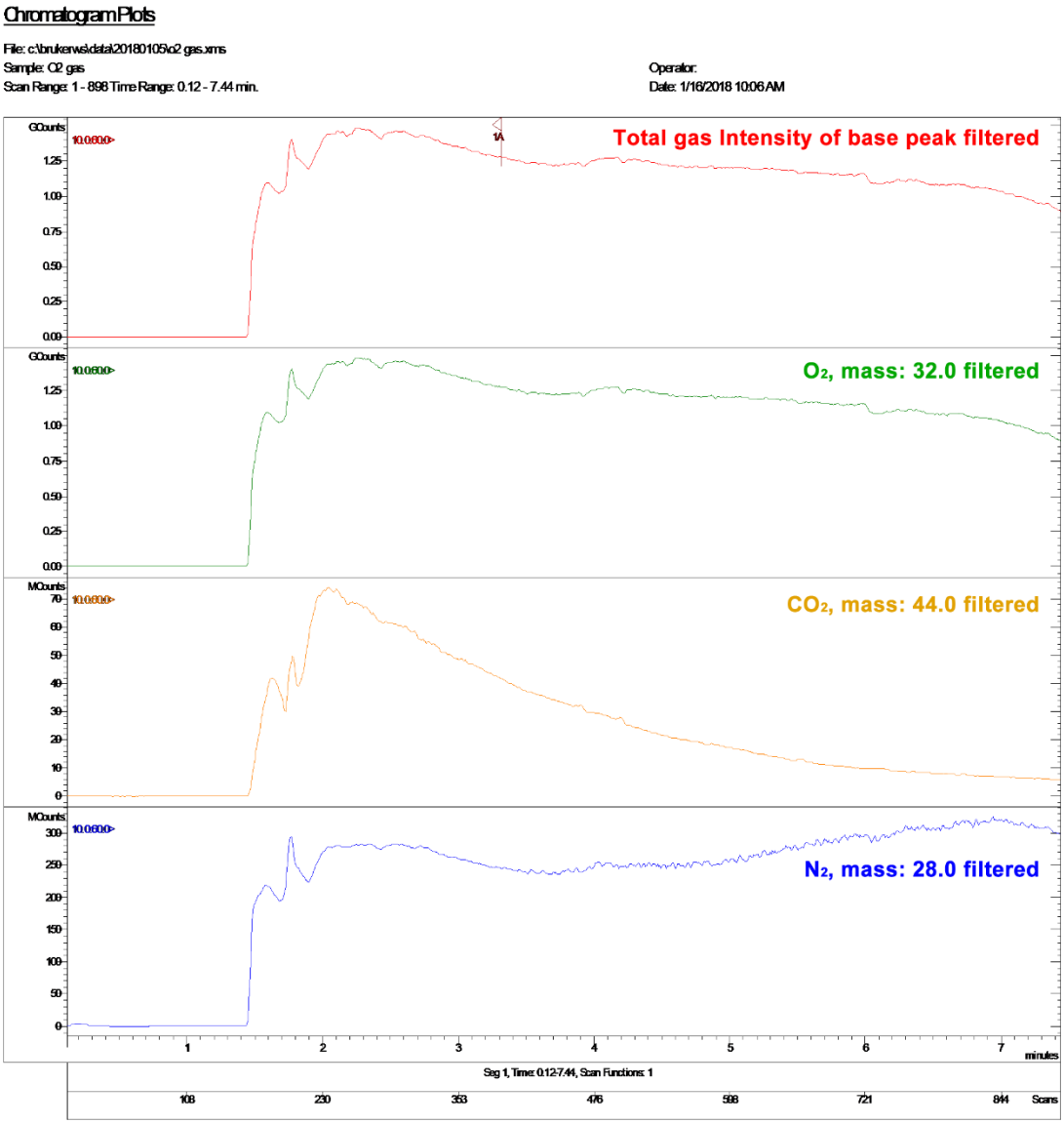

Figure S10. Raw data of gas chromatography profiles of evolved gas during charging process. Related to Figure S9 and Figure 4. As shown in **Figure S9**, the GC profile reveals the gas contains O_2, CO_2, N_2. This raw data of GC intensity profiles is obtained and total gas, and each gas component profiles are indicated. The total gas is obtained in order of GCounts (1.25×10^9). For O_2, it obtained in almost same intensity (1.25×10^9). For CO_2, however, the intensity is obtained in 7.0×10^7, revealing the intensity is significantly smaller than that of O_2 (~ 2 order difference). Because the measuring is conducted in CO_2 purged aqueous electrolytes, the dissolved CO_2 could be generated. In the case of N_2, a bit more intensity is obtained in 3.0

$\times 10^8$. Since N_2 cannot be produced in any electrochemical oxidation reactions, it is arisen from the inflow of air during measuring process. Therefore, the evolved gas during charging process is confirmed to be O_2.

Table S1. Concentration of various ions when CO_2 dissolves in water at normal atmospheric pressure. Related to Figure 1.

pCO_2 (atm)	$[CO_2(aq)]$ (mol L^{-1})	$[H_2CO_3(aq)]$ (mol L^{-1})	$[HCO_3^-(aq)]$ (mol L^{-1})	$[CO_3^{2-}(aq)]$ (mol L^{-1})	$[H^+(aq)]$ (mol L^{-1})	pH
3.5×10^{-4}	1.18×10^{-5}	1.41×10^{-8}	2.29×10^{-6}	4.69×10^{-11}	2.29×10^{-6}	5.64

Table S2. Comparison of various batteries capacity. Related to Figure 3.

	Current density (mA g^{-1})	Catalyst loading (mg cm^{-2})	Gravimetric capacity (mAh g^{-1})	Area specific capacity (mAh cm^{-2})
This work	**200**	**2**	**210,000**	**420**
Li-CO_2 battery (Zhang et al., 2015)	50	0.27-0.45	14,723	6.5
Li-CO_2 battery (Qie et al., 2017)	300	0.3	16,006	4.8
Na-CO_2 battery (Hu et al., 2016)	1,000	0.071	60,359	42.9
Na-CO_2 battery (Das et al., 2013)	70	0.76-1.28	3,478	4.5
Mg-CO_2 battery (Al Sadat and Archer, 2016)	70	0.76-1.28	2,540	3.3
Al-CO_2 battery (Al Sadat and Archer, 2016)	70	0.5-1.0	13,322	13.3
Li-O_2 battery (Kang et al., 2006)	280	0.72	11,060	8.0
Li-ion battery (Wang et al., 2012)	280	6.66	225	1.5

Transparent Methods

Half-cell configured electrochemical analysis.

In three-electrode half-cell measurements, a platinum wire was used as both of working electrode and counter electrode with Ag/AgCl (saturated KCl filled) reference electrode in 0.1 M sodium hydroxide (NaOH, Sigma-Aldrich Co.) in pure water and seawater (taken from sea of Ulsan and filtered to remove visible impurities). To estimate pH and hydrogen evolution potential in the solution, a reversible hydrogen electrode (RHE) calibration was conducted in H_2-saturated solutions where platinum wires were used as the working, counter electrodes and Ag/AgCl as a reference electrode at a scan rate of 1 mV s^{-1}. For all half-cell configured experiments, iR correction was applied by measuring the resistance of solution (0.1 M NaOH, CO_2-saturated 0.1 M NaOH, seawater, CO_2-saturated seawater). The ohmic resistances of before CO_2-saturated 0.1 M NaOH, after CO_2-saturated 0.1 M NaOH, before CO_2-saturated seawater, and after CO_2-saturated seawater have been confirmed as 12.5, 35.8, 4.2 and 4.0 Ω, respectively. A rotating disk electrode testing was conducted by using a mixture of 20wt.% Pt/C and IrO_2 catalyst (Sigma-Aldrich Co., mixed in 1 : 1 gravimetric ratio) on RRDE-3A (ALS Co.). The mixture of catalyst was prepared into a catalyst ink by dispersing 10 mg of the catalyst in 1 mL of a binder solution (45 : 45 : 10 = ethanol : isopropyl alcohol : 5 wt.% Nafion solution (Sigma-Aldrich Co.), volumetric ratio) followed by a bath sonication process. The oxidation RDE profiles were measured by 5 μL of the catalyst ink drop-coated glassy carbon disk electrode, where area is 0.1256 cm^2, at a scan rate of 10 mV s^{-1}. All electrochemical tests were carried out using Biologic VMP3.

Characterization techniques.

The soluble solid products after discharge process in CO_2-saturated 0.1 M NaOH were obtained through various drying process such as freeze-drying, natural drying at room-temperature, high temperature drying at 70°C oven. The phase identification of the obtained products was

confirmed by X-ray powder diffraction (XRD) (Bruker diffractometer, Cu Kα radiation) at a scan rate of 1^{o} min^{-1}. The power patterns were analyzed using JADE 6.5 software. The generated gas from discharge process was collected using three-electrode configuration in CO_2-saturated seawater and 0.1 M NaOH by water substitution method using U tube. Then the gas was analyzed by gas chromatograph (Agilent 7820A GC instrument) with a thermal conductivity detector (TCD) and a packed column (Agilent carboxen 1000). The gas used for GC measurement were controlled using a mass flow controller (MFC) (Atovac GMC1200) and the exact volume value of gas was calibrated through a bubble flow meter. The gas evolved from the charging process were also collected by three-electrode configuration (Pt wires as a counter electrode, Pt/C+IrO_2 catalyst loaded carbon felt as a working electrode, and Ag/AgCl as a reference electrode) in 0.1 M NaOH. The gas was analyzed by 450-GC chromatograph and 320-MS (Bruker Co.). The morphological analysis of the working electrode before and after discharge process in hybrid Na-CO_2 system was examined by scanning electron microscopy (Nova FE-SEM, FEI Co.).

Full-cell measurements.

For testing the hybrid Na-CO_2 system, the commercial Na-air battery (seawater battery) system was purchased at 4TOONE Co. and we modified the system into hybrid Na-CO_2 system. The hybrid Na-CO_2 system is composed of Na metal / organic electrolyte / solid electrolyte / aqueous electrolyte / cathode. For the organic electrolyte, 1 M Sodium trifluoromethanesulfonate ($NaCF_3SO_3$, Sigma-Aldrich Co.) in tetraethylene glycol dimethyl ether (TEGDME, Sigma-Aldrich Co.) was used. And NASICON-type (NASICON: Na super ionic conductor) $Na_3Zr_2Si_2PO_{12}$ with a thickness of 1 mm and a diameter of 16 mm was used as the solid electrolyte. The anode coin cell was assembled in Ar-filled glove box where the water and oxygen concentrations were kept less than 1 ppm. The sodium metal (Sigma-Aldrich Co.) with a diameter of 16 mm and a thickness of 0.5 mm was loaded on the stainless-steel

metal support and the prepared organic electrolyte was filled between sodium metal and NASICON. After assembling the anode coin cell with proper sealing, the assemblage was moved out from the glove box. The assembled coin cell is 24 mm in diameter and 6.5 mm in thickness (2465 size). For the aqueous electrolyte, 150 mL of 0.1 M NaOH and seawater were used. The cathode was prepared by drop-coating the catalyst ink (Pt/C+IrO_2 ink) in a carbon felt electrode (Fuel Cell Store Co.) with a loading density of 2 mg cm^{-2}. The current density was normalized with the loading density of the catalysts. A titanium wire was used as a current collector of the cathode and the aqueous electrolytes were saturated by CO_2 at a rate of 50 mL min^{-1} at the ambient air condition for electrochemical measurements in hybrid Na-CO_2 system. All electrochemical tests were conducted using Biologic VMP3.

References

Zhang, Z., Zhang, Q., Chen, Y., Bao, J., Zhou, X., Xie, Z., Wei, J., and Zhou, Z. (2015). The first introduction of graphene to rechargeable Li-CO_2 batteries. Angew. Chem. Int. Ed. *54*, 6550-6553.

Qie, L., Lin, Y., Connell, J.W., Xu, J., and Dai, L. (2017). Highly rechargeable lithium-CO_2 batteries with a boron- and nitrogen-codoped holey-graphene cathode. Angew. Chem. Int. Ed. *56*, 6970-6974.

Hu, X., Sun, J., Li, Z., Zhao, Q., Chen, C., and Chen, J. (2016). Rechargeable room-temperature Na-CO_2 batteries. Angew. Chem. Int. Ed. *55*, 6482-6486.

Das, S.K., Xu, S., and Archer, L.A. (2013). Carbon dioxide assist for non-aqueous sodium-oxygen batteries. Electrochem. Commun. *27*, 59-62.

Al Sadat, W. I., and Archer, L.A. (2016). The O_2-assisted Al/CO_2 electrochemical cell: A system for CO_2 capture/conversion and electric power generation. Sci. Adv. *2*, e1600968.

Kang, K., Meng, Y. S., Bregėr, J., Grey, C. P., and Ceder, G. (2006). Electrodes with high power and high capacity for rechargeable lithium batteries. Science *311*, 977-980.

Wang, Z.-L., Xu, D., Xu, J.-J., Zhang, L.-L., and Zhang, X.-B. (2012). Graphene oxide gel-derived, free-standing, hierarchically porous for high-capacity and high rate rechargeable Li-O_2 batteries. Adv. Funct. Mater. *22*, 3699-3705.